






## Optimizing Donor Cellular Dissociation and Subretinal Injection Parameters for Stem Cell-Based Treatments

BRITNI A. SCRUGGS <sup>a</sup>, CHUNHUA JIAO,<sup>a</sup> CATHRYN M. CRANSTON,<sup>a</sup> EMILY KAALBERG,<sup>a</sup> KAI WANG,<sup>b</sup> STEPHEN R. RUSSELL,<sup>a</sup> LUKE A. WILEY,<sup>a</sup> ROBERT F. MULLINS,<sup>a</sup> EDWIN M. STONE,<sup>a</sup> BUDD A. TUCKER <sup>a</sup>, ELLIOTT H. SOHN <sup>a</sup>

**Key Words.** Induced pluripotent stem cells • Retinal progenitor cells • Stem cell transplantation • Subretinal transplantation • Inherited retinal dystrophy • Pig model

<sup>a</sup>University of Iowa Institute for Vision Research and the Department of Ophthalmology and Visual Sciences, University of Iowa, Iowa City, Iowa, USA;

<sup>b</sup>Department of Biostatistics, College of Public Health, University of Iowa, Iowa City, Iowa, USA

Correspondence: Elliott H. Sohn, M.D., University of Iowa Hospitals and Clinics, Institute for Vision Research, 200 Hawkins Drive, Iowa City, Iowa 52242, USA. Telephone: 319-356-2864; e-mail: elliott.sohn@gmail.com

Received September 27, 2018; accepted for publication March 7, 2019; first published April 19, 2019.

<http://dx.doi.org/10.1002/sctm.18-0210>

This is an open access article under the terms of the Creative Commons Attribution-NonCommercial-NoDerivs License, which permits use and distribution in any medium, provided the original work is properly cited, the use is non-commercial and no modifications or adaptations are made.

### ABSTRACT

Subretinal delivery of stem cell-derived retinal cells as a strategy to treat retinal degenerative blindness holds great promise. Currently, two clinical trials are underway in which human fetal retinal progenitor cells (RPCs) are being delivered to patients by intravitreal or subretinal injection to preserve or restore vision, respectively. With the advent of the induced pluripotent stem cell (iPSC), and in turn three-dimensional derivation of retinal tissue, it is now possible to generate autologous RPCs for cell replacement. The purpose of this study was to evaluate the effect of commonly used cell isolation and surgical manipulation strategies on donor cell viability. iPSC-RPCs were subjected to various conditions, including different dissociation and isolation methods, injection cannula sizes, and preinjection storage temperatures and times. The effects of commonly used surgical techniques on both host and donor cell viability were evaluated in Yucatan mini-pigs ( $n = 61$  eyes). We found a significant increase in cell viability when papain was used for RPC isolation. In addition, a significant decrease in cell viability was detected when using the 41G cannula compared with 31G and at storage times of 4 hours compared with 30 minutes. Although 96.4% of all eyes demonstrated spontaneous retinal reattachment following injection, retinal pigment epithelium (RPE) abnormalities were seen more frequently in eyes receiving injections via a 31G cannula; interestingly, eyes that received cell suspensions were relatively protected against such RPE changes. These findings indicate that optimization of donor cell isolation and delivery parameters should be considered when developing a subretinal cell replacement strategy. *STEM CELLS TRANSLATIONAL MEDICINE* 2019;8:797–809

### SIGNIFICANCE STATEMENT

Subretinal delivery of viral vectors and stem cells will be essential to treat the outer retina in patients with blinding, inherited eye diseases. However, there are scant data to support the optimal conditions for preparing and injecting induced stem cell-derived retinal precursor cells for transplantation. This study examined (a) in vitro cell preparation conditions to determine their impact on pretransplantation cell viability and (b) the surgical outcomes of various parameters in live Yucatan pigs receiving subretinal vehicle or retinal precursor cells. The results demonstrate that the needle cannula size, storage time, incubation temperature, and injection rate impact cell viability and surgical outcomes. This study suggests that the optimization of subretinal injections will improve the chances of restoring vision in patients with retinal degenerative diseases.

### INTRODUCTION

Over the past decade, a significant body of the literature has been amassed to demonstrate the potential of stem cell-based cell replacement for the treatment of retinal degenerative blindness [1–5]. To restore vision in patients with advanced, rare inherited retinal disorders such as retinitis pigmentosa [6], new photoreceptor cells

will be required. For patients with more common genetically complex diseases such as age-related macular degeneration [7–10], in addition to photoreceptor cells, replacement of both retinal pigment epithelium (RPE) and choroidal endothelial cells may be needed.

As long-term systemic immunosuppression will likely be required to maintain transplants containing cells that are not immunologically

matched to the host, the ideal donor cell source for retinal cell replacement is the autologous patient-derived induced pluripotent stem cell (iPSC) [11]. Like embryonic stem cells (ES), iPSCs can be differentiated into any cell type from any of the three embryonic germ layers, including photoreceptor cells, RPE cells, and choroidal endothelial cells. Although extensive data exist to demonstrate that iPSC-derived retinal cells have the ability to integrate with the remaining host retina [6, 12–14], different strategies for retinal cell replacement have resulted in variable success. For instance, nonautologous iPSC-derived RPE cell transplants can result in minimal clinical adverse effects, but elicit an immune response at the cellular level in various animal models [15–17]. On the other hand, autologous RPE transplantation studies in humans have resulted in retinal detachment, ocular inflammation, proliferative vitreoretinopathy, and/or hemorrhage post-transplantation [18–21]. These various approaches demonstrate some of the challenges that must be addressed before cell transplantation may restore vision in a meaningful way with acceptable risk to these patients.

Supplementing our understanding through animal experimentation, several trials have focused on transplantation of ES-derived and iPSC-derived RPE cells for the treatment of AMD [8, 15, 22–27]. A unifying theme of these trials has been that delivery of stem cell-derived RPE cells in suspension is inferior to transplantation of RPE cells as an organized sheet (RPE cell graft) [7, 28–30]. Specifically, unlike RPE cell grafts, which following subretinal transplantation lay flat and integrate with the remaining host RPE cell layer, many of the dissociated RPE cells injected into the subretinal space may be lost due to efflux and apoptosis. The donor cells that do survive fail to adhere to Bruch's membrane and elaborate into an organized physiologic monolayer [31]. Similar findings have been reported in preclinical animal studies focused on stem cell-based photoreceptor cell replacement. Specifically, as compared with cell suspension injection, retinal progenitor cells (RPCs) transplanted into the subretinal space on polymeric cell support scaffolds results in an approximately ninefold increase in donor cell survival [32]. This finding can largely be attributed to apoptosis due to a loss of cellular adhesion (anoikis), and to physical shear force stresses associated with cellular dissociation and direct injection via small gauge cannulas. The observations in recent reports have demonstrated that photoreceptor precursor cells directly isolated from developing mouse retina and transplanted into diseased hosts results in extensive donor cell death with transfer of donor cell material to remaining host photoreceptor cells, further suggesting that stem cell-derived progeny are fragile and will be more successfully transplanted on a prefabricated biomimetic graft rather than as a cellular slurry. By dissociating cells during early retinal differentiation and seeding them onto a cell delivery scaffold [33] where they will be allowed to mature and adhere prior to transplantation, one can mitigate acute cellular dissociation effects and maximize post-transplant cell viability. Moreover, although retinal graft transplantation is our ultimate goal, early stage clinical trials designed to evaluate both safety and efficacy of intravitreal and subretinal injection of a suspension of human RPCs in patients are currently underway (clinicaltrials.gov numbers NCT02464436 and NCT03073733). As such, evaluation of the effects of various donor cell isolation, storage, and delivery parameters on cell viability is timely.

Interestingly, there is a paucity of published data on the methodology and safety of subretinal injections or the effects of transplantation conditions on both donor and host cell viability. For instance, the ideal injection rate to avoid harming residual host RPE cells and overlying retina is uncertain. It is also unclear how the size of the injection cannula used affects retinal reattachment without air–fluid exchange and the cellular effects on the RPE [34]. The porcine eye is an excellent model for preclinical development of a retinal cell replacement strategy and in particular testing of these surgical injection parameters. Like humans, the pig has a multilayered retina with a cone-rich region called the visual streak with similarities to the human macula. In addition, as the pig eye is closer in size to that of the human, one can develop surgical approaches using instruments and techniques that can be readily translated to human retinal surgery.

We and others have previously demonstrated the ability to (a) identify the specific genetic mutations responsible for causing various inherited eye diseases in our patients [35–38]; (b) generate patient-derived iPSCs and correct their disease causing mutations using the CRISPR-Cas9 system [39]; (c) differentiate iPSCs into retinal cells using good manufacturing practices (GMP) [5, 40]; and (d) transplant allogenic iPSC-derived photoreceptor or RPE cells into a large animal model using pars plana vitrectomy [15] and subretinal injections [15, 25]. The goals of this study were twofold: first, we sought to optimize our donor cell dissociation methods in an attempt to isolate the maximum number of healthy RPCs from three-dimensional (3D) retinal organoids that could be delivered for seeding of retinal cell grafts; second, we sought to characterize and optimize the subretinal injection parameters used for creating a subretinal bleb prior to retinal graft transplantation. To do so, we analyzed outcomes from several key components of surgery, including retinal reattachment with variably sized needle-cannulas and the effect of injection rate on retinal morphology. In addition, we compared injections with saline to those with a slurry of donor cells and assessed viscosity changes and growth factors that may potentially protect host cells from damage. We believe that improving postdissociation cell viability and surgical outcomes in the pig model will translate to safer, more effective therapy to patients with retinal degenerative diseases.

## MATERIALS AND METHODS

### Generation of Patient-Derived iPSCs and Retinal Organoids

Three-millimeter skin biopsies were obtained from patients with known inherited retinal disease. Fibroblast cells were isolated and expanded prior to being used for iPSC generation via overexpression of SOX2, C-MYC, KLF4, and OCT4 as described previously [37, 41, 42]. Passage 10 iPSCs were karyotyped and analyzed using the scorecard assay [5]. Validated iPSCs were subsequently subjected to our previously published 3D retinal differentiation protocol [5]. Briefly, iPSCs were passaged, counted, and plated at a density of  $1 \times 10^4$  cells per well in 96-well conical bottom, low attachment plates in 3D differentiation media to induce sphere formation [5]. At 12 days postplating, spheres were transferred to ultra-low attachment cell culture dishes and fed with neural retina (NR) differentiation media every other day. At ~30 days postdifferentiation, retinal tissue was dissected free from the attached forebrain tissue and cultured as retinal organoids until harvest.

### Dissociation of 3D Retinal Organoids for Isolation of RPCs

3D retinal organoids differentiated for 60 days were thoroughly minced using a sterile razor blade in NR differentiation media. A 1 ml pipette was used to transfer the minced tissue into a 15 ml conical tube. The cell culture plate, in which the retinal organoids were minced, was washed twice with fresh NR media, which was added to the conical tube following each wash to avoid losing cells (this is especially important around the periphery of the dish). The cell suspension was triturated using a fire polished pasture pipette and subsequently centrifuged at 300g for 5 minutes at room temperature (RT). Supernatant was removed and the cell pellet was resuspended in dissociation media (Papain [Sigma–Aldrich, St. Louis, MO] 20 U/ml and DNase I [Invitrogen, Carlsbad, CA] 10 U/ml in NR differentiation media) at a density of two organoids per milliliter. Tubes were subsequently incubated for 25–30 minutes in a 37°C water bath with gentle, intermittent agitation. Following incubation, approximately 5 ml of Dulbecco's modified Eagle's medium containing 10% human serum was added and the suspension was centrifuged at 300g for 5 minutes at RT. Following centrifugation, the supernatant was removed and the cell pellet was re-suspended in balanced salt solution (BSS)/Hanks' buffered salt solution (HBSS) buffer (Fisher Scientific, Pittsburgh, PA) at a concentration of approximately ~10,000 cells per microliter. If reconstituted for plating purposes, the cell pellet was suspended in NR differentiation media supplemented with RevitaCell (Thermo Fisher Scientific, Waltham, MA).

### Immunocytochemical Staining of Dissociated RPCs

Dissociated RPCs (isolated from retinal organoids differentiated for 60 days) were plated in a four-chamber cell culture slide coated with laminin overnight at 4°C. At 4 days postplating, the cells were fixed in 4% paraformaldehyde for 5 minutes, blocked using immunoblock, and stained using the primary antibodies melanogenesis-associated transcription factor (MITF; Exalpa Biologicals, Shirley, MA), Pax6 (BioLegend, San Diego, CA), Sox2 (R&D Systems, Minneapolis, MN), Nanog (R&D Systems, Minneapolis, MN), NRL (R&D Systems, Minneapolis, MN), and OTX2 (R&D Systems, Minneapolis, MN) and the secondary antibodies Cy2, Cy3, Cy5, and Alexa-488. DAPI was used as a counterstain. Images were obtained using an EVOS XL cell imaging system.

### Cell Viability Studies

RPCs were injected through polyamide cannulas of different gauges (31G versus 41G, MedOne Surgical, Inc., Sarasota, FL). Noninjected cells were also exposed to various incubation temperatures (0°C, 21°C, 37°C, and 50°C) after varying lengths of storage time (30 minutes versus 4 hours). Cell viabilities were determined using a tetrazolium (MTS) assay and/or a Countess II FL Automated Cell Counter (Invitrogen). The cell viabilities were determined immediately after injection. MTS Cell Proliferation Assay Kit (Abcam, Cambridge, MA) was used according to the manufacturer's instructions and the formazan dye product was quantified by measuring the absorbance at 490–500 nm. For the trypan blue quantification, the percentage of recovered, live cells per sample was calculated using a Countess II FL Automated Cell Counter (Invitrogen) and verified using a hemocytometer after exposure to trypan blue.

### Animals and Animal Testing

All animal procedures were approved by the Institutional Animal Care and Use Committee of the University of Iowa and conducted in accordance with the ARVO Statement for the Use of Animals in Ophthalmic and Vision Research. Three to 6-months-old nonimmune suppressed wild-type Yucatan miniature swine (Sinclair Bio-resources; Auxvasse, MO) were obtained ( $n=31$  pigs). Anesthesia was induced using ketamine 5 mg/kg, dexmedetomidine 0.03 mg/kg, and butorphanol 0.3 mg/kg given intramuscularly by a registered veterinarian technician and maintained at 0.5%–5% isoflurane. The pupils were dilated with 1% tropicamide ophthalmic solution (Alcon, Inc.; Lake Forest, IL) followed by 2.5% phenylephrine hydrochloride ophthalmic solution (Paragon; Portland, OR). An endotracheal tube was placed with the SpO<sub>2</sub> and heart rate monitored continuously throughout the procedure. The pigs were placed in either the right or left lateral decubitus position. A lateral canthotomy was performed to increase exposure of the eye. To keep the number of animals used to a minimum, subretinal injections were performed in both eyes of each animal ( $n=61$  eyes).

### Pars Plana Vitrectomy and Subretinal Injections of RPCs into a Pig Model

Animals were prepped and draped in typical sterile fashion for ophthalmic surgery with an eyelid retractor placed appropriately. Cellugel (Alcon; Fort Worth, TX) or hypromellose 2.5% ophthalmic demulcent solution (OCuSoft, Inc.; Rosenberg, TX) was applied to the cornea during the procedure for ocular lubrication. A conjunctival peritomy was performed to expose the sclera. Three pars plana sclerotomies with 23-gauge trocars were made approximately 1.5–2 mm posterior to the limbus. A BSS enriched with bicarbonate, dextrose, and glutathione (BSS Plus; Fort Worth, TX) was infused into the eye throughout the procedure to maintain a pressure of approximately 20 mmHg. After a posterior vitreous detachment was induced, a polyamide cannula (31G or 41G, MedOne Surgical, Inc.; Sarasota, FL) was used to create a small retinotomy to inject 300 µl of a vehicle solution ( $n=41$  eyes), or 3 million human iPSC-RPCs ( $n=20$  eyes) directly into the subretinal space of the cone-rich visual streak region. For the vehicle injections using the 31G cannula, there were five buffers tested as these have been used by various research groups in animals and human trials utilizing gene therapy vectors: BSS ( $n=5$ ), BSS Plus ( $n=5$ ), buffer A with N-acetylcysteine (NAC;  $n=5$ ), buffer A without NAC ( $n=5$ ), and HBSS ( $n=10$ ); buffer A represents a buffer commonly used for human subretinal injections that consists of 180 mM sodium chloride and 10 mM sodium phosphate at a pH of 7.2. For the vehicle injections using the 41G cannula, BSS was injected ( $n=11$ ).

The cannula was inserted through the retina between the optic nerve and visual streak to result in a bleb in the subretinal space. Cannulas were removed and sclerotomies were sutured with 7-0 vicryl suture. Air–fluid exchange was not performed on any eye in the study. A single intravitreal injection of 1 mg/0.025 cc triamcinolone was administered to all eyes that received subretinal injection via the larger, 31G, cannula. The operative eye was then bathed with 5% povidone-iodine. For pigs that received cells, the first eye was injected with the cell solution and the second eye was immediately injected with vehicle. Indirect ophthalmoscopy was performed at sacrifice on post op week 2 to post op week 5 to detect retinal

reattachment and RPE changes. For euthanasia, pigs were given intramuscular ketamine (14 mg/kg) and intramuscular acepromazine (1 mg/kg). The eyes were dilated and an eye exam was performed. Blood was taken via an ear vein. Euthasol (1 ml/10 lbs) was then given intravenously. Vitreous was collected after both eyes were enucleated.

### Tissue Processing and Histological Procedure

All eyes were enucleated at designated time points and processed for histological assessment. In brief, whole eyes were immediately fixed in 4% fresh paraformaldehyde overnight then processed and embedded in paraffin for morphologic analysis as described previously [15]. Transverse 10  $\mu$ m serial paraffin sections from central disc toward the superior periphery were collected and mounted on Superfrost Plus glass slides. Every 200  $\mu$ m of sections were deparaffinized and stained with hematoxylin and eosin (H&E) for overall morphological assessment. Selected adjacent sections were used for immunohistochemistry staining using double-label or triple-label immunofluorescence techniques. After deparaffinization, sections were blocked in 2% bovine serum albumin in phosphate-buffered saline. Primary antibodies (e.g., anti-RPE65 or anti-IgG antibodies) were then applied to sections. Secondary antibodies were conjugated to Alexa fluorochromes 488, 568, or 594 (1:200, Thermo Fisher). Sections were rinsed and counterstained with DAPI then analyzed and imaged with an Olympus BX41 fluorescence microscope.

### Injection Rate Studies and Morphometry Analysis

Domestic cadaveric pig eyes obtained from a local abattoir within 4 hours after enucleation underwent vitrectomy as described above for the *in vivo* surgeries. Subretinal injection of 300  $\mu$ l of BSS buffer was administered at 1.8 ml/minute ( $n=8$ ) or 0.18 ml/minute ( $n=6$ ) using an automated syringe pump injector (New Era Pump System). Control eyes underwent vitrectomy without subretinal injection ( $n=4$ ). Both non-injected and injected eyes were processed as described above. At every 200  $\mu$ m, tissue sections were assessed for the presence of a bleb and depigmented RPE (i.e., pseudo-geographic atrophy; pseudo-geographic atrophy [GA], described below). A subset of adjacent sections was then selected and immunolabeled with an anti-RPE65 antibody (Novus International, St Charles, MO, dilution 1:100) overnight at 4°C, followed by a 1 hour incubation in Cy3-conjugated secondary antibody (Jackson Immuno Research Lab, West Grove, PA). Antifade medium with DAPI was used for counterstaining and coverslipping. All images were captured along the entire length of the bleb with an Olympus BX41 fluorescence microscope. To measure RPE65 loss, multiple images across the entire bleb were automatically photo merged in Photoshop (Adobe Photoshop CS, Adobe Systems, San Jose, CA); Fiji-Image J software was used to measure both the length of bleb and the missing RPE65 layer length. The ratio of RPE65 signal loss was calculated by the absence of RPE65 over total length of bleb in every 20th section (i.e., every 200  $\mu$ m).

### Multiplex Porcine Cytokine/Chemokine Assay

Supernatant was obtained from 34 pig eye vitreous samples following euthanasia either 2 weeks or 5 weeks after subretinal injections of various buffers (BSS, BSS Plus, buffer A with NAC, buffer A without NAC, and HBSS) with or without the intraoperative use of preservative-free triamcinolone acetate.

A total of 25  $\mu$ l of each neat vitreous supernatant was loaded in duplicate and tested with the Milliplex Porcine Cytokine/Chemokine Magnetic Bead Panel (Millipore, PCYTMG-23K-13PX, Temecula, CA) according to the manufacturer's instructions. To obtain the supernatant, all vitreous samples were centrifuged at 12,000 rpm at 4°C for 15 minutes, then the supernatant snap frozen in liquid nitrogen and stored at -80°C until use. For any given treatment group, protein from 5 to 10 pig eyes was tested in duplicate with each well representing a single eye. The concentrations of cytokines/chemokines were measured and analyzed according to the manufacturer's protocol on a BioRad Bio-plex 200 Suspension Array System with Bio-Plex Manager 5.0 software (Bio-Rad Laboratories, Hercules, CA). All reported values were calculated based on the standard curve of each individual plate.

### Statistical Analysis

All *in vitro* injection conditions were tested in three independent experiments in triplicate using pooled cells isolated from five patients with known inherited retinal disease. For the cell viability studies, histological studies, *in vivo* studies, and injection rate studies, statistical analysis of three or more groups was performed using one-way analysis of variance (ANOVA) followed by pairwise comparisons of the groups using post hoc testing with Bonferroni correction. To determine the interaction between temperature and time, two-way ANOVA was performed with Sidak's comparisons testing. Statistical analyses with a two-tailed Student's *t* test was used for comparison of only two means. Retinal reattachment and postoperative data were analyzed by Pearson chi-square test then Fisher's exact test. Logistic regression was used to determine if the presence of vitreous opacities on exam was associated with elevated cytokine levels and if there were any significant covariates, including week of sacrifice, use of triamcinolone, and presence of pseudo-GA. For all cytokines analyzed, no significant covariates were identified; therefore, Pearson chi-square test and Fisher's exact test were used. Significance for the overall group effect and individual pairwise comparisons was defined as  $p < .05$  for all experiments. Logistic regression analyses were performed by MedCalc for Windows, version 18.0 (MedCalc Software, Ostend, Belgium). All other statistical tests and graphs were performed using GraphPad Prism 4.0b for Macintosh (GraphPad Software, San Diego, CA), and all values were reported as mean  $\pm$  SEM except the cytokine experiments, which reported values as median with range.

## RESULTS

### RPC Isolation and Characterization

RPCs were isolated from iPSC-derived 3D retinal organoids as described in Materials and Methods (Fig. 1A). Postdissociation RPC viability (i.e., percentage of recovered, live cells) was  $98.40\% \pm 2.78\%$  using a MTS assay at RT (Fig. 2B). RPCs were isolated using papain attached to laminin-coated plates by 1 day postplating and began to spread across the culture surface by day 4 (Fig. 1A). As previously reported, RPE precursor cells began to lose their dark pigment, which was present at day 1, and adopted a more fibroblastic morphology [37, 43] (Fig. 1A, arrows). Immunocytochemical analysis demonstrated that cultures contained cells that expressed the retinal cell transcription factor PAX6, the RPC markers SOX2 and OTX2



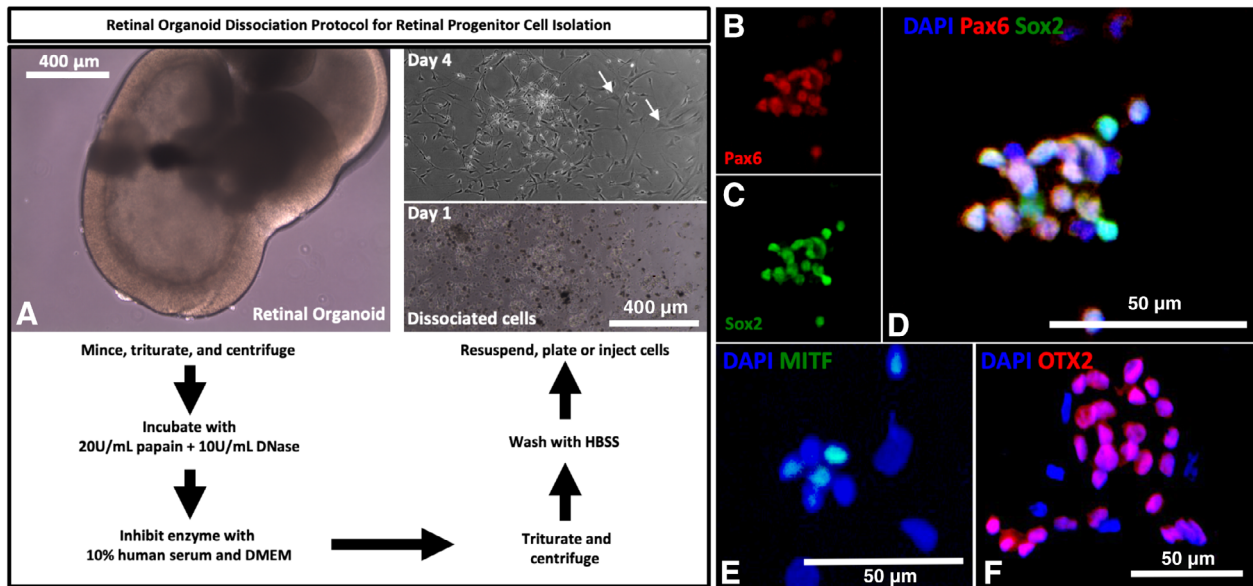


**Figure 1.** Isolation of retinal progenitor cells from three-dimensional (3D) retinal organoids. **(A):** Retinal progenitor cells were isolated from 3D retinal organoids (via the protocol outlined in the schematic) and plated on laminin-coated culture surfaces at 60 days postdifferentiation via papain dissociation. At 1 day postplating, a mix of pigmented RPE and nonpigmented neural retinal progenitor cells were present. By 4 days postplating, cells began to spread over the culture surface (a loss of pigment was noted at this time point). Scale bar: 400 μm. **(B–F):** Immunocytochemical analysis targeted against Pax6 (B, D), Sox2 (C, D), MITF (E), and OTX2 (F) revealed the presence of retinal progenitor and RPE cell precursors, respectively. Scale bar: 50 μm. Abbreviations: DAPI, 4',6-diamidino-2-phenylindole; MITF, melanogenesis-associated transcription factor; OTX2, orthodenticle homeobox 2; Pax6, paired box 6; Sox2, SRY (sex determining region Y)-box 2.

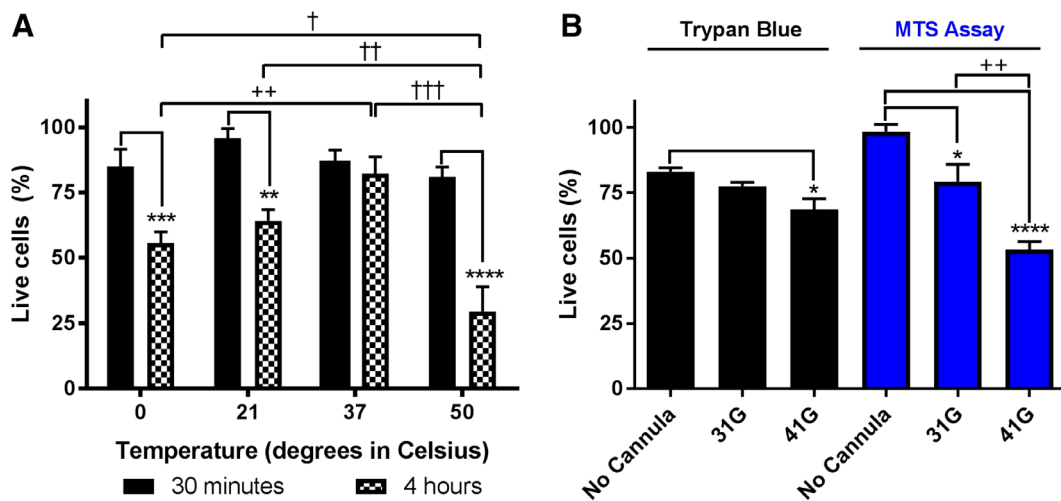


**Figure 2.** Temperature, storage time, and cannula gauge effect retinal progenitor cell viability. **(A):** Induced pluripotent stem cell-derived retinal progenitor cells (RPCs) were incubated at various temperatures (0°C, 21°C, 37°C, and 50°C). Cell viabilities (mean ± SEM) were measured using trypan blue staining and an automatic cell counter after 1 hour (black) and 4 hours (checked). Two-way ANOVA was performed (factors: temp and time) with Sidak's comparisons testing. \*\*,  $p < .01$ ; \*\*\*,  $p < .001$ ; \*\*\*\*,  $p < .0001$  comparing temperature-matched samples. ++,  $p < .01$  comparing 37° to 0° at 4 hours. †,  $p < .05$ ; ††,  $p < .01$ ; †††,  $p < .001$  comparing samples to 50° at 4 hours. **(B):** RPCs were injected through either a larger cannula (31G) or a smaller cannula (41G) and collected for in vitro analysis of the percentage of live cells compared with preinjection cell counts. Cell viabilities (mean ± SEM) were measured immediately using an automatic cell counter using trypan blue staining (black) or an MTS assay (blue). \*,  $p < .05$ ; \*\*,  $p < .01$ ; \*\*\*\*,  $p < .0001$  compared with no cannula. ††,  $p < .01$  comparing 31G to 41G. Abbreviations: G, gauge of needle-cannula; MTS, tetrazolium assay.

and the RPE cell transcription factor MITF (Fig. 1B–1F). Cultures did not express the pluripotency transcription factor Nanog nor did they express the rod photoreceptor precursor cell transcription factor NRL (data not shown). Collectively, these data demonstrate that cultures isolated from 3D retinal

organoids at 60-days postdifferentiation contain a mixture of neural retinal progenitor and RPE precursor cells, similar to those delivered to humans in two independent clinical trials that are currently underway (ClinicalTrials.gov numbers NCT02464436 and NCT03073733).

**Table 1.** Indirect ophthalmoscopic postoperative findings after subretinal injection of either vehicle or induced pluripotent stem cell-derived retinal precursor cells using 41G or 31G needle-cannulas

| Postoperative findings<br>(no. of eyes/total<br>no. of eyes examined) <sup>b</sup> | 41G cannula           |           |           | 31G cannula           |          |             |                          |                            |           |           | <i>p</i> values <sup>a</sup> |                     |
|--|-----------------------|-----------|-----------|-----------------------|----------|-------------|--------------------------|----------------------------|-----------|-----------|------------------------------|---------------------|
|  | Cells                 |           | Vehicle   | Cells                 |          | Vehicle     |                          |                            |           |           | Cells vs.<br>vehicle         | 31G vs.<br>41G      |
|  | iPSC-derived<br>cells | BSS       | Total     | iPSC-derived<br>cells | BSS      | BSS<br>Plus | Buffer<br>A <sup>c</sup> | Buffer A<br>without<br>NAC | HBSS      | Total     |                              |                     |
| Spontaneous retinal reattachment   | 10/10                 | 10/11     | 95.2%     | 6/6                   | 5/5      | 4/5         | 4/4                      | 5/5                        | 9/9       | 97.1%     | >.9999                       | >.9999              |
| Pseudo-GA  | 1/10                  | 5/8       | 33.3%     | 0/6                   | 3/5      | 3/4         | 2/3                      | 4/5                        | 2/9       | 43.8%     | *.0007 <sup>d</sup>          | .5558               |
| All RPE changes  | 2/10                  | 5/8       | 38.9%     | 4/6                   | 3/5      | 3/4         | 2/3                      | 5/5                        | 7/9       | 75%       | *.0272 <sup>e</sup>          | *.0165 <sup>f</sup> |
| Vitreous opacities   | 3/10                  | 5/9       | 42.1%     | 6/9                   | 3/5      | 0/4         | 2/5                      | 2/5                        | 3/9       | 43.2%     | .7765                        | >.9999              |
| Retinal fold   | 6/10                  | 2/8       | 44.4%     | 0/6                   | 0/5      | 0/4         | 1/4                      | 2/5                        | 1/9       | 12.1%     | .1573                        | *.0153 <sup>g</sup> |
| Uveitis  | 0/10                  | 0/11      | 0%        | 2/8                   | 1/5      | 0/4         | 1/4                      | 0/5                        | 0/9       | 11.4%     | .5866                        | .2856               |
| Total eyes injected ( <i>n</i> )   | <b>10</b>             | <b>11</b> | <b>21</b> | <b>10</b>             | <b>5</b> | <b>5</b>    | <b>5</b>                 | <b>5</b>                   | <b>10</b> | <b>40</b> |                              |                     |

<sup>a</sup>Postoperative data were analyzed by chi-square test and then Fisher's exact test. Significance was defined as  $p < .05$  (indicated by \*).

<sup>b</sup>For all postoperative observations, the total number of eyes provided is the number of eyes that could be adequately examined for that particular postoperative finding. Media opacities and/or surgical complications (e.g., total cataract, total retinal detachment, etc.) limited assessment of retinal pathology for several eyes.

<sup>c</sup>Buffer A represents a buffer commonly used for human subretinal injections that consists of 180 mM sodium chloride and 10 mM sodium phosphate at a pH of 7.2.

<sup>d</sup>When controlling for cannula size, the *p* values are \*.0430 and \*.0238 for the 41G and 31G groups, respectively.

<sup>e</sup>There was no statistical difference between the 31G versus 41G groups when controlling for injection type.

<sup>f</sup>When controlling for injection type, the *p* values are \*.0338 and .6021 for the cell and vehicle groups, respectively.

Abbreviations: BSS, balanced salt solution; G, gauge of needle-cannula; GA, geographic atrophy; HBSS, Hanks' balanced salt solution; iPSC, induced pluripotent stem cells; NAC, N-acetylcysteine; RPE, retinal pigment epithelium.

### Effects of Injection Conditions on in vitro Cell Viability

Patient-derived RPCs were subjected to various conditions in vitro, including different temperatures, incubation time, and cannula size (Fig. 2). To investigate the effects of temperature and incubation time on cell viability, RPCs were incubated at 0°C, 21°C, 37°C, and 50°C with cell viabilities measured using an automated cell counter after 30 minutes and 4 hours. Two-way ANOVA was performed, a significant interaction between temperature and time was found with Sidak's comparisons testing ( $F[3, 38] = 5.835$ ;  $p = .002$ ). There was no significant difference between the temperature groups when cell viability was measured at 30 minutes. However, the incubation time significantly affected the cell viability across all groups ( $F[1,38] = 54.93$ ;  $p < .0001$ ). When these samples were incubated for 4 total hours, the 37°C incubation group had significantly increased cell viabilities compared with the group incubated on ice ( $p < .01$ ; Fig. 2A). Furthermore, the 0°C ( $p < .001$ ), 21°C ( $p < .01$ ), and 50°C ( $p < .0001$ ) groups all had significant decreases in the cell viabilities compared with their 30 minute counterparts (Fig. 2A). In contrast, the 37°C group had stable values over time. As expected, the 0°C ( $p < .05$ ), 21°C ( $p < .01$ ), and 37°C ( $p < .001$ ) groups had significantly higher cell viabilities when compared with the 50°C control group (Fig. 2A).

To study the effect of cannula size on progenitor cell viability, these cells were injected at 1 million cells per 100  $\mu$ l through a 41G (smaller) or 31G (larger) cannula (Fig. 2B). Trypan blue staining, followed by automated cell counting, was initially used for this purpose, but the trypan blue was found to be mildly toxic to the cells with only 83.00%  $\pm$  1.58% of the cells surviving in the control group, where no cannula was used (Fig. 2B). This method did demonstrate a significant decrease in cell survival when using the smaller cannula

(68.6%  $\pm$  4.12% live cells) compared with no cannula ( $p < .05$ ; Fig. 2B). A MTS assay that used colorimetric analysis of metabolically active cells was found to be more sensitive and compatible with cell health. Using the MTS assay, 98.40%  $\pm$  2.78% of the cultured cells survived the assay when no cannula was used. The cell viability decreased to 79.33%  $\pm$  6.52% when the RPCs were injected through the 31G cannula ( $p < .05$ ; Fig. 2B). However, there was a decline to 53.32%  $\pm$  3.12% cell survival when using the 41G cannula ( $p < .0001$ ; Fig. 2B). Comparison of these cell viabilities between the 31G and 41G cannula groups was significant ( $p < .01$ ; Fig. 2B). These in vitro results represent three independent experiments in triplicate using cells isolated from five patients.

### Ophthalmoscopy and Histological Analysis of Pig Eyes Following Subretinal Bleb Formation

To raise a subretinal bleb (that would also be suitable for retinal cell graft implantation), following pars plana vitrectomy, a polyamide cannula (31G or 41G) was used to inject BSS ( $n = 41$  eyes) directly into the subretinal space of the cone-rich visual streak region. Indirect ophthalmology was performed for all pig eyes ( $n = 41$ ) at the time of sacrifice either at post op week 2 or post op week 5 to detect retinal reattachment and to record all postoperative findings, including: "pseudo-GA" (used to describe the clinical appearance of a focal sharply demarcated region of RPE depigmentation with or without true histological RPE atrophy), RPE changes without GA, vitreous floaters/opacities, retinal folds, uveitic processes, cataract formation, and corneal opacities. The number of affected eyes per category was compared between those that received injections via 41G versus 31G-cannulas. Table 1 provides an overview of these indirect ophthalmoscopic postoperative findings.

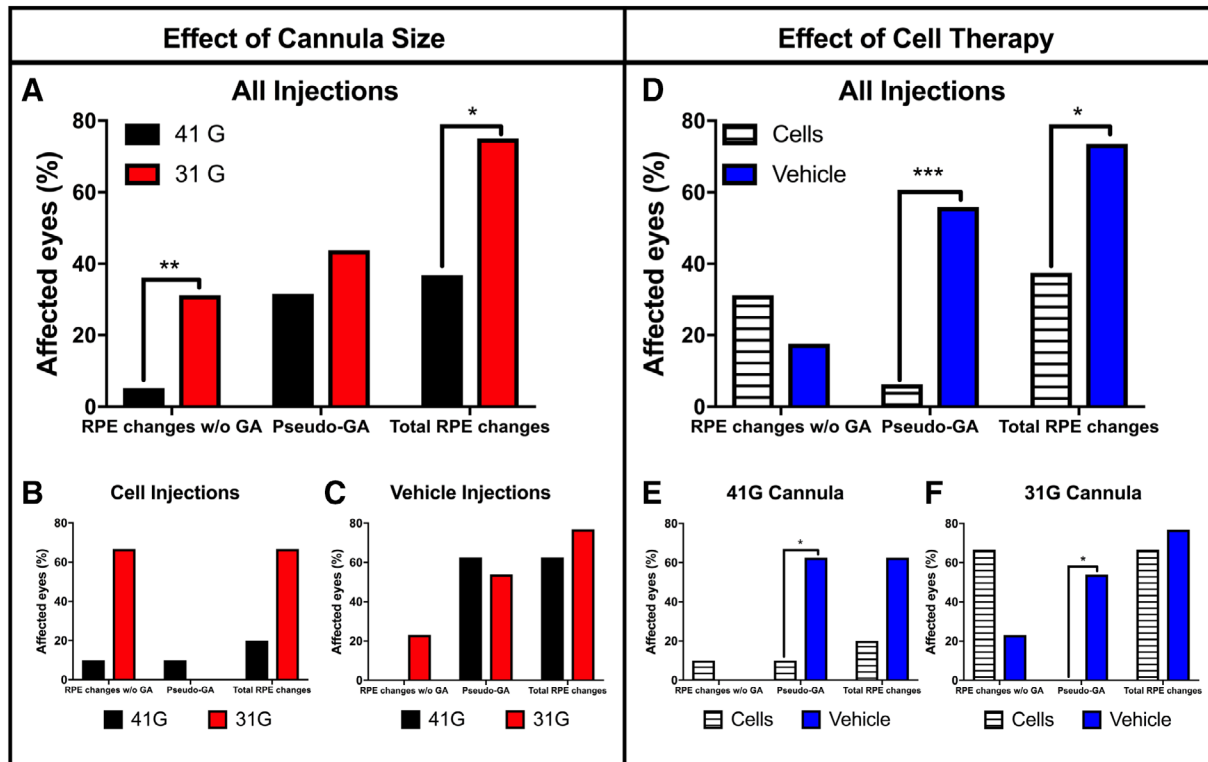


**Figure 3.** Statistical analysis of injection conditions in association with pseudo-geographic atrophy or RPE changes based on ophthalmoscopic assessment. Indirect ophthalmoscopy was performed on all eyes ( $n = 50$ ) that received subretinal injections of either iPSC-derived retinal progenitor cells ( $n = 16$ ) or vehicle ( $n = 34$ ) via a 31G ( $n = 32$ ) or 41G cannula ( $n = 18$ ), and the number of eyes with pseudo-GA or RPE changes without GA were compared between the two cannula groups (A–C) or the two injection groups (D–F). For (A)–(C), comparisons between the cannula groups were performed for all eyes that received subretinal injections (A), eyes that only received iPSC-derived RPC injections (B), and eyes that only received subretinal vehicle injections (C). For (D)–(F), the number of eyes with pseudo-GA or RPE changes were compared between the two treatment groups for all eyes that received subretinal injections (E), eyes that only received 41G cannula injections (F), and eyes that only received 31G cannula injections (G). For each graph, bars represent the percentage of affected eyes for a specific finding. Data were analyzed by chi-square test and then Fisher’s exact test using GraphPad prism software.  $p < .05$  was considered statistically significant. All eyes that were examined and found to have a dense cataract, total retinal detachment, and/or dense vitreous opacities were excluded as the presence or absence of pseudo-GA and RPE could not be assessed. Abbreviations: G, gauge of needle-cannula; GA, geographic atrophy; RPE, retinal pigment epithelium. \*,  $p < .05$ ; \*\*\*,  $p < .001$ .

Dense media opacities ( $n = 1$ ), total cataracts ( $n = 3$ ), and uveitis with anterior chamber fibrin, hypopyon, or small pupil ( $n = 2$ ) limited assessment of retinal pathology for six eyes. There were eight eyes with very mild, focal cataracts and seven eyes that had diffuse, mild corneal edema; neither of these findings impacted the analysis of other postoperative findings. Of the eyes that had an adequate view to the retina, 96.4% of these pig eyes (53 out of 55) had spontaneous retinal reattachment using the 31G (33 out of 34 eyes) and 41G (20 out of 21 eyes) cannulas (Table 1). Hematoxylin and eosin stain was performed on some nonimmune suppressed pigs injected with human iPSC-derived RPCs (Supporting Information Fig. S2), but extensive phenotyping was not done as these xenografts would be expected to result in more robust cellular immune reaction than we reported in 2015 when allogeneic cells in the subretinal space led to an activated adaptive immune response [15].

We compared the effects of cannula size on the presence of RPE abnormalities (i.e., RPE changes without GA, pseudo-GA, and total RPE changes). The 31G cannula group had an increased amount of RPE changes without GA ( $p = .009$ ) and total RPE changes ( $p = .017$ ) compared with the 41G cannula

group (Fig. 3A); however, the 31G-injected eyes were not associated with increased amount of pseudo-GA ( $p = .56$ ). When controlling for the type of injection (i.e., cells or vehicle only), there was no difference between any of the RPE abnormalities between the cannula groups (Fig. 3B, 3C).

We also performed statistical analyses to determine the effect of iPSC-RPCs (which might increase fluid viscosity) on the incidence of RPE changes with or without GA (Fig. 3D–3F). The iPSC-derived cell-injected eyes had a significantly decreased amount of pseudo-GA compared with the vehicle-injected group ( $p < .001$ ; Fig. 3D). When controlling for the type of cannula used, there was still less pseudo-GA in the cell-injected cohort using 41G ( $p = .043$ ; Fig. 3E) or 31G ( $p = .024$ ; Fig. 3F) cannulas. Comparing these same groups for RPE changes without GA, there was no difference between the cell and vehicle groups ( $p > .99$ ; Fig. 3D). Of the 26 eyes that received vehicle through a 31G cannula, the number of eyes with pseudo-GA or significant RPE changes was compared with determined effect of buffer type. All vehicle-injected groups had eyes with pseudo-GA, but the HBSS group had fewer eyes with pseudo-GA (two out of nine) compared with the buffer A group with NAC (four out of five;  $p = .036$ ); otherwise, there



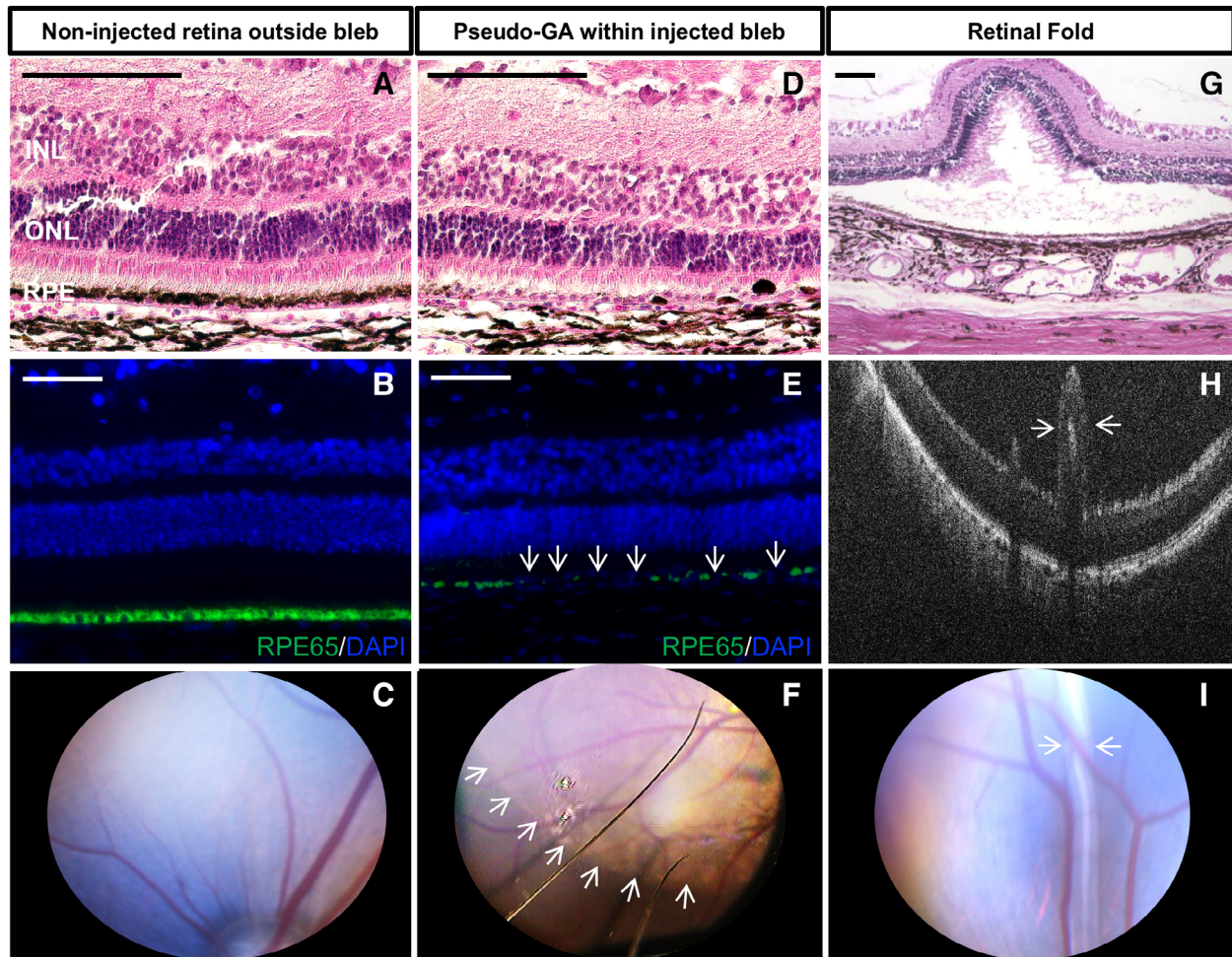


**Figure 4.** Histological and clinical evidence of pseudo-GA and retinal folds after subretinal vehicle injections in a pig model. (A–C): Representative images taken outside the bleb region (i.e., noninjected retina). (D–I): Representative images taken of the injected, bleb region of these eyes show evidence of either pseudo-GA (D–F) or retinal folds (G–I). The images in (A), (B), (D), and (E) represent the same eye. H&E staining (A and D) shows depigmentation of the retinal pigment epithelium within the bleb region only (D), and immunohistochemistry (B and E) demonstrates that this same bleb region has a significant loss (E, white arrows) of RPE65 signal (green). For (B) and (E), DAPI was used to counterstain nuclei. Indirect ophthalmoscopy demonstrates a normal appearance of the retina outside the bleb region (C) and RPE changes with pseudo-GA within the bleb region (F, white arrows). (G–I): A prominent retinal fold within the bleb region is seen using H&E staining (G), ocular coherence tomography imaging (H, white arrows), and indirect ophthalmoscopy (I, white arrows). Scale bar = 100  $\mu$ m. All panels are from postoperative week 2 except (C) (postoperative week 1), (F) (week 5) and (I) (week 1). Abbreviations: DAPI, 4',6-diamidino-2-phenylindole; GA, geographic atrophy; INL, inner nuclear layer; ONL, outer nuclear layer; RPE, retinal pigment epithelium; RPE65, retinal pigment epithelium marker.

was no significant difference between the postoperative findings of the various buffer groups.

There was no significant difference in the number of eyes with vitreous opacities or uveitis when comparing the 31G versus 41G cannula groups or the cell-injected versus vehicle-injected groups (Table 1). There were a higher number of eyes in the 41G cohort (44.4%) that developed retinal folds compared with the 31G cohort (12.1%,  $p = .015$ ; Table 1). We identified these prominent retinal folds within the bleb region using H&E staining (Fig. 4G), ocular coherence tomography imaging (Fig. 4H), and indirect ophthalmoscopy (Fig. 4I); Figure 4G–4I images represent three different pig eyes in the 41G cannula group. Of note, there was no difference in retinal fold incidence between eyes receiving cells versus vehicle ( $p = .16$ ).

To determine the effects of these subretinal vehicle injections on the integrity of the retina, the post-mortem pig eyes were processed for histological analysis of the retinal layers.

Eight eyes with pseudo-GA seen on exam (Fig. 4F) were evaluated histologically (Fig. 4D) and compared with eyes without clinical pseudo-GA (Fig. 4A). The RPE was intact in all eight eyes; however, there was depigmentation of the apical villi in five eyes, and there was also irregular loss of RPE65 expression in three eyes, as determined by immunofluorescence staining (Fig. 4E). These were no eyes that had positive IgG staining (data not shown). Representative images of these experiments are shown in Figure 4. The retina and underlying RPE regions outside the injected bleb appeared normal histologically (Fig. 4A, 4B); however, in the same eye, the bleb region was found to have profound RPE depigmentation (Fig. 4D) with significant loss of RPE65 expression (Fig. 4E, white arrows). Fundus images were obtained of regions outside the injected region (Fig. 4C) and within the bleb region (Fig. 4F, white arrows) to demonstrate the striking appearance of pseudo-GA we appreciated in many of the eyes injected with vehicle.



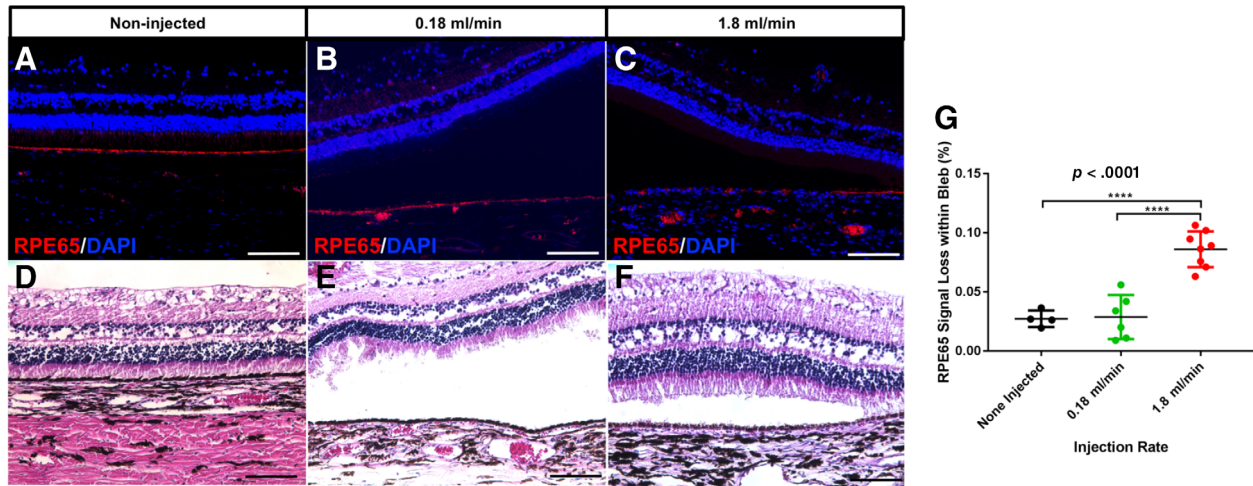


**Figure 5.** Differential effects of injection rate on loss of RPE65 expression in cadaver pig eyes. (A–C): RPE65 retinal pigment epithelial cell marker-immunolabeled (red) histological sections show higher expression of RPE65 in noninjected vitrectomized pig cadaver eyes (A;  $n = 4$ ) compared with 1.8 ml/minute injected eyes (C;  $n = 8$ ) but not to 0.18 ml/minute injected eyes (B;  $n = 6$ ). Nuclei were counterstained with DAPI (blue). (D–F): Corresponding H&E stains on adjacent sections (bottom panels) show no substantial change in pigmentation of RPE in the 1.8 ml/minute group (F) compared with noninjected vitrectomized control sections (D) and the lower 0.18 ml/minute injection group (E). Scale bar: 100  $\mu\text{m}$ . (G): There was a significant loss of RPE65 signal in the pig retinas injected with at a high speed (1.8 ml/minute) compared with the retinas injected at a lower speed (0.18 ml/minute) and the retinas that were not injected. Each point represents the percentage of RPE65 signal loss for the bleb region of an individual eye, and inset horizontal lines show results as mean  $\pm$  SEM.  $p < .05$  was considered statistically significant. For all histological images, representative images are shown. Abbreviations: DAPI, 4',6-diamidino-2-phenylindole; RPE65, retinal pigment epithelium marker.

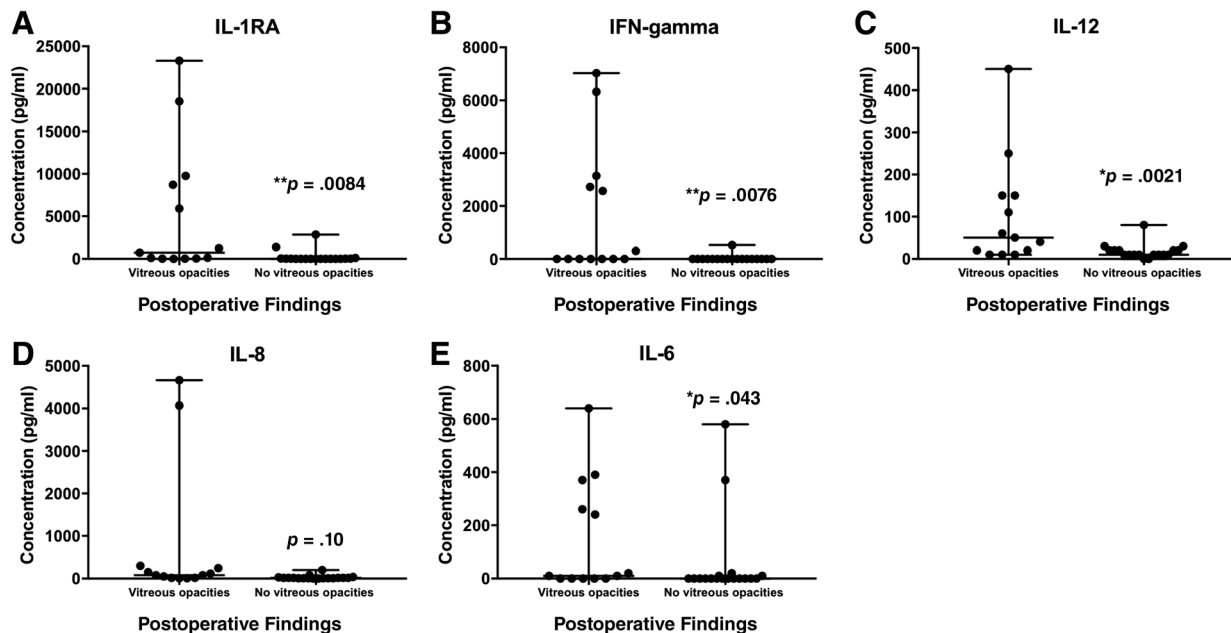


**Figure 6.** Upregulated inflammatory cytokine levels in pig eyes with vitreous floaters/opacities after subretinal vehicle injections. (A–E): Analysis of inflammatory cytokines by multiplex analysis. Supernatant was obtained from pig vitreous samples at euthanization 2–5 weeks after subretinal injections. These samples were analyzed on a 13-plex panel multiplex plate, which confirmed that at least five inflammatory mediators (IL-1RA, IFN- $\gamma$ , IL-12, IL-8, and IL-6) are upregulated in the vitreous at the protein level for eyes with ophthalmoscopic evidence of vitreous floaters. Each point represents the average of duplicate readings of the cytokine concentration in an individual eye, and inset horizontal lines show results as median with range. Concentrations lower than the low limit of detection were defined as nonmeasurable, and data were analyzed by chi-square test and then Fisher’s exact test. Logistic regression analyses were also performed and there were no significant covariates.  $p < .05$  was considered statistically significant. Abbreviations: IL, interleukin; IFN, interferon.

**Effects of Injection Rate on Retinal Histology**

To determine the effect of injection rate on RPE and surrounding tissue, fresh cadaveric pig eyes were injected at a speed of 1.8 ml/minute ( $n = 8$ ) or 0.18 ml/minute ( $n = 6$ ) then processed

for qualitative and quantitative assessment by H&E staining and immunostaining (Fig. 5). Analysis of immunohistochemistry (Fig. 5A–5C) and H&E imaging (Fig. 5D–5F) demonstrated the loss of RPE65 immunolabeling but no effect on RPE

depigmentation, respectively, in the eyes that received the faster injection (Fig. 5). When compared with the ex vivo vitrectomized cadaver eyes without injection, there was no statistical difference in H&E images or RPE65 signal when compared with the slower rate at 0.18 ml/minute (Fig. 5G). However, there was a marked decline in RPE65 signal when comparing the control group ( $2.7\% \pm 0.4\%$ ,  $n=4$ ,  $p < .0001$ ) or the slower rate ( $2.9\% \pm 0.8\%$ ,  $p < .0001$ ) to the higher injection rate ( $8.6\% \pm 0.5\%$ ,  $p < .0001$ ; Fig. 5G).

### Vitreous Cytokine Levels in Eyes Receiving Subretinal Vehicle Injections

To help elucidate the mechanism for some of the postoperative changes seen, we measured the level of 13 cytokines in vitreous samples from eyes that received subretinal vehicle with ( $n=7$ ) or without ( $n=26$ ) the use of preservative-free triamcinolone acetonide, which was administered at the end of cases utilizing 31G needles to help reduce postoperative intraocular inflammation. These vitreous samples were obtained at the time of sacrifice, either at post op week 2 ( $n=26$ ) or post op week 5 ( $n=7$ ). Of the 13 cytokines tested, there were four cytokines, IL-2, IL-4, IL-18, and TNF- $\alpha$ , that were not detectable in any tested sample. IL-1  $\alpha$ , IL-1  $\beta$ , IL-10, and GM-CSF were detectable in some but not the majority of eyes tested. Most vitreous samples had cytokine levels above the level of detection (LOD) for interferon (IFN)  $\gamma$ , IL-1RA, IL-6, IL-8, and IL-12. Interestingly, for these five highly detectable cytokines, there were two to seven eyes per cytokine that had relatively high values. In order to investigate this further, we identified all the eyes that were noted on postoperative exam to have vitreous floaters/opacities and then compared the cytokine levels between eyes that had floaters versus eyes that had no vitreous opacities. Chi-square testing was performed to compare the number of samples with cytokine levels over the LOD between the groups. There was a significant upregulation of IFN- $\gamma$  ( $p = .008$ ), IL-1RA ( $p = .008$ ), IL-6 ( $p = .043$ ), and IL-12 ( $p = .021$ ) in the eyes with post op vitreous opacities (Fig. 6). There was no significant correlation between the presence of vitreous opacities and the presence of pseudo-GA, the use of intraoperative triamcinolone, or the timing of exam (Supporting Information Fig. S1).

## DISCUSSION

Our laboratory previously demonstrated that (a) iPSC-derived photoreceptor precursor cells integrate within the outer retina of retinal degeneration mouse models [37] and that (b) transplantation on polymeric cell support scaffolds is superior to cell injection alone [44]. Herein, we describe the isolation of patient-derived RPCs from 3D retinal organoids at 60-days postdifferentiation. Our ultimate goal is to use these cells for loading of photoreceptor cell delivery scaffolds, which following further maturation in culture to induce photoreceptor precursor cell fate commitment, may be used for autologous cell replacement based treatment of patients with advanced retinal degenerative blindness. All steps of the 3D retinal differentiation protocol used in this study were described previously and performed in accordance with current GMP [41]. Unlike earlier 2D differentiation protocols, in which it was difficult to separate retinal from nonretinal forebrain tissue, by using this

3D retinal differentiation approach we can readily generate and isolate RPCs in the absence of contaminating forebrain neurons (for method, refer [41]). In addition, by isolating cells from retinal organoids that are differentiated for 60 days, we are able to largely avoid contamination of inner retinal ganglion cells, which are born much earlier and largely lost by this time point due to lack of nutrient and oxygen exchange afforded to the innermost layers of the enlarged organoid [41]. Following generation, we have described an effective dissociation protocol that allows us to consistently isolate RPCs for retinal cell graft production without compromising cell yield. These cells are expected to be very similar to those used in the above-described ongoing clinical trials, which are isolated during retinal development from human fetal retina. As indicated above, our ultimate goal is to use 3D retinal organoid derived RPCs to generate engineered photoreceptor precursor cell grafts rather than use these cells as a direct therapy for photoreceptor cell replacement. In light of ongoing clinical trials, we reasoned that it would be useful to provide an evaluation of cellular isolation and surgical manipulation parameters that may impact both host and donor cell viability. To that end, in this study we demonstrate how needle cannula size, pretransplantation cell storage time, cell incubation temperature, and solution injection rate impact cell viability and surgical outcomes. These data indicate that if a single cell retinal cell transplantation approach is to be used it should be promptly timed after cell preparation, and delays in transplantation warrant incubation of these cells at 37°C, which may not be routine practice for many stem cell biologists.

The purpose of cell transplantation for retinal degenerative diseases is to provide healthy cells to replace degenerated ones of the outer retina and/or RPE. However, the process of preparing cell suspensions and delivering these cells directly to the intended region has the potential to negatively affect cell number and/or cell integrity. Although many vitreoretinal surgeons prefer to perform subretinal injections using the smallest cannula size possible, our study suggests that larger cannulas result in better cell viability without an increased risk of retinal detachment, despite the larger hole necessary to subretinally deliver the cells. This expands on a recent paper by Wilson et al., in which 30G cannulas were found to be superior to 41G cannulas for optimization of cell recovery and viability [45].

We use the term "pseudo-GA" in this manuscript to distinguish it from true GA, which is the defining feature of advanced nonexudative age-related macular degeneration that consists of irreversible RPE, photoreceptor, and choroidal loss similarly identified in humans on fundus examination [46–48]. The use of the term GA would be problematic for describing the findings in our study without further investigation as: (a) we did not find morphologic evidence of surrounding photoreceptor or choroidal loss in histologic sections and (b) it is unknown if the RPE disturbance identified may resolve over time (i.e., at least one study suggests this possibility after RPE damage in pigs [34]).

The injection rate/cell viability relationship we have found, indicates the importance of controlling injection rate for subretinal bleb formation for the purpose of retinal cell graft transplantation and cell suspension delivery when choosing this intervention paradigm. To demonstrate the importance of injection rate for subretinal bleb formation, we injected vehicle solutions into the subretinal space of fresh cadaver pig

eyes; when injecting at a higher, controlled speed, there are significant RPE changes and disruption of the outer retina when compared with the same buffers injected at slower speeds. RPE cells, although intact morphologically, have a corresponding loss of RPE65 signal associated with increased speed of injection. This loss of RPE65 is also identified in manually injected pig eyes 2 to 5 weeks following surgery. These findings are especially important when injecting manually through a larger cannula, as we postulate that the 31G cannula injections induced more RPE changes than the smaller cannula due to the increased lumen size and increased volume injected per time, which is independent of the type of buffer injected. RPE changes and depigmentation with subretinal injections has been described previously [49, 50], and we hypothesize that this may occur at higher incidence in the larger cannula 31G group due to a turbulence effect that is exacerbated with higher injection speed. The decreased pseudo-GA seen in eyes injected with cells may be due to less turbulence and trauma to the RPE from increased fluid viscosity. Although the mechanism of action needs further studies to confirm these findings, at this time we recommend surgeons inject at a lower, controlled rate for subretinal injections of any fluid.

Wilson et al. recently described the presence of transplanted cells and debris in the vitreous samples after transvitreal transplantation [45]. We, too, observed an egress of fluid from the retinotomy site into the vitreous cavity. Although this fluid loss ultimately decreases the number of cells transplanted, data suggest that this fluid egress may protect the bleb from increased retinal strain that leads to the development of retinal folds such as those that we saw in the 41G cannula group. For all human cell-injected pig eyes that developed uveitis or had vitreous opacities on exam, we considered these reactions a result of xenogeneic cells introduced into the vitreous cavity. However, there was no significant difference in the frequency of media opacities when comparing the cell and vehicle groups, and, in fact, 41% of all vehicle-injected eyes had prominent vitreous opacities. Although tempting to think vitreous opacities could be secondary to triamcinolone debris, the clinical picture of vitreous triamcinolone did not appear similar to these opacities and our cytokine data suggest that even vehicle-injected eyes have a robust inflammatory reaction. Based on our data, we do not believe the vitreous inflammation we encountered is a result of the buffer used, the triamcinolone injected, or the surgical techniques implemented. We observed a trend of decreasing vitreous opacities and cytokine levels 5 weeks following surgery, and this is consistent with the transient mild ocular inflammation seen in the phase III trial using subretinal injections of gene therapy for RPE65-mediated inherited retinal dystrophy [51]. This suggests that immunosuppression in the initial period after transplantation may be necessary for clinical trials involving subretinal injections for gene and stem cell treatments (regardless of donor cell source).

## CONCLUSION

Our data support the hypotheses that patient-specific RPCs can be isolated from iPSC-derived 3D-retinal organoids, and the viability of these cells can be improved by optimizing dissociation parameters and postdissociation conditions such as temperature, cannula gauge, and storage time. Both 31G and

41G cannulas can be used to successfully administer subretinal injections that will spontaneously reattach without need for long-acting gas or laser in pigs. Higher bleb injection speeds result in RPE changes or pseudo-GA seen postoperatively that correlates to RPE depigmentation and loss of RPE65 expression. Postoperative vitreous opacities and increased cytokine production were the most common adverse effects associated with subretinal injection/retinal bleb formation. The findings from this study have broad applicability to treatments that rely on subretinal injections, such as gene therapy and bolus stem cell-derived retinal cell transplantation.

## ACKNOWLEDGMENTS

This work was supported by University of Iowa Institute for Vision Research Endowment, NEI R01-EY026547, P30 EY025580, Lidsky/Zawadzki/McGuinn/Cohen Families, Hope for Vision, VitreoRetinal Surgery Foundation (VRSF), and the Howard F. Ruby Endowment for Human Retinal Engineering. We thank Erin Burnight, Ph.D., Kristin Anfinson, B.A., Tasneem Putliwala, Ph.D., and Kristan Worthington, Ph.D. at the University of Iowa for their instruction, advice, and suggestions regarding the *in vitro* and *in vivo* studies. We also thank the rest of the veterinary and vivarium staff of the University of Iowa Animal Facility for the daily care of the pigs. We thank Zuhair Ballas, M.D. and Justin Fishbaugh of the University of Iowa Flow Cytometry Facility for their assistance with the cytokine detection assay.

## AUTHOR CONTRIBUTIONS

B.A.S.: conception and design, collection and/or assembly of data, data analysis and interpretation, manuscript writing; C.J.: conception and design, collection and/or assembly of data, data analysis and interpretation; C.M.C.: collection and/or assembly of data, data analysis and interpretation; E.K.: collection and/or assembly of data; K.W., S.R.R.: data analysis and interpretation; L.A.W.: collection and/or assembly of data, data analysis and interpretation; R.F.M.: data analysis and interpretation, manuscript writing; E.M.S.: data analysis and interpretation, administrative support; B.A.T.: conception and design, financial support, administrative support, data analysis and interpretation, manuscript writing, final approval of manuscript; E.H.S.: conception and design, collection and/or assembly of data, financial support, administrative support, data analysis and interpretation, manuscript writing, final approval of manuscript.

## DISCLOSURE OF POTENTIAL CONFLICTS OF INTEREST

E.H.S. declared research funding from Oxford Biomedica; Sanofi; Regeneron. S.R.R. declared research funding from Spark Therapeutics and ProQR and is a consultant to Novartis. The other authors indicated no potential conflicts of interest.

## DATA AVAILABILITY STATEMENT

The data that support the findings of this study are available from the corresponding author upon reasonable request.



## REFERENCES

- 1 Klassen HJ, Ng TF, Kurimoto Y et al. Multipotent retinal progenitors express developmental markers, differentiate into retinal neurons, and preserve light-mediated behavior. *Invest Ophthalmol Vis Sci* 2004;45:4167–4173.
- 2 MacLaren RE, Pearson RA, MacNeil A et al. Retinal repair by transplantation of photoreceptor precursors. *Nature* 2006;444:203–207.
- 3 Bartsch U, Oriyakhel W, Kenna PF et al. Retinal cells integrate into the outer nuclear layer and differentiate into mature photoreceptors after subretinal transplantation into adult mice. *Exp Eye Res* 2008;86:691–700.
- 4 Santos-Ferreira T, Völkner M, Borsch O et al. Stem cell-derived photoreceptor transplants differentially integrate into mouse models of cone-rod dystrophy. *Invest Ophthalmol Vis Sci* 2016;57:3509–3520.
- 5 Wiley LA, Burnight ER, DeLuca AP et al. cGMP production of patient-specific iPSCs and photoreceptor precursor cells to treat retinal degenerative blindness. *Sci Rep* 2016;6:30742.
- 6 Wiley LA, Burnight ER, Songstad AE et al. Patient-specific induced pluripotent stem cells (iPSCs) for the study and treatment of retinal degenerative diseases. *Prog Retin Eye Res* 2015;44:15–35.
- 7 Mandai M, Kurimoto Y, Takahashi M. Autologous induced stem-cell-derived retinal cells for macular degeneration. *N Engl J Med* 2017;377:792–793.
- 8 Li Y, Tsai YT, Hsu CW et al. Long-term safety and efficacy of human-induced pluripotent stem cell (iPS) grafts in a preclinical model of retinitis pigmentosa. *Mol Med* 2012;18:1312–1319.
- 9 Songstad AE, Wiley LA, Duong K et al. Generating iPSC-derived choroidal endothelial cells to study age-related macular degeneration. *Invest Ophthalmol Vis Sci* 2015;56:8258–8267.
- 10 Nazari H, Zhang L, Zhu D et al. Stem cell based therapies for age-related macular degeneration: The promises and the challenges. *Prog Retin Eye Res* 2015;48:1–39.
- 11 Takahashi K, Tanabe K, Ohnuki M et al. Induction of pluripotent stem cells from adult human fibroblasts by defined factors. *Cell* 2007;131:861–872.
- 12 Wright LS, Phillips MJ, Pinilla I et al. Induced pluripotent stem cells as custom therapeutics for retinal repair: Progress and rationale. *Exp Eye Res* 2014;123:161–172.
- 13 Viczian AS. Advances in retinal stem cell biology. *J Ophthalmic Vis Res* 2013;8:147–159.
- 14 Tucker BA, Mullins RF, Stone EM. Stem cells for investigation and treatment of inherited retinal disease. *Hum Mol Genet* 2014;23:R9–R16.
- 15 Sohn EH, Jiao C, Kaalberg E et al. Allogenic iPSC-derived RPE cell transplants induce immune response in pigs: A pilot study. *Sci Rep* 2015;5:11791.
- 16 McGill TJ, Stoddard J, Renner LM et al. Allogenic iPSC-derived RPE cell graft failure following transplantation into the subretinal space in nonhuman primates. *Invest Ophthalmol Vis Sci* 2018;59:1374–1383.
- 17 Carr AJ, Vugler AA, Hikita ST et al. Protective effects of human iPSC-derived retinal pigment epithelium cell transplantation in the retinal dystrophic rat. *PLoS One* 2009;4:e8152.
- 18 Maaijwee K, Heimann H, Missotten T et al. Retinal pigment epithelium and choroid translocation in patients with exudative age-related macular degeneration: Long-term results. *Graefes Arch Clin Exp Ophthalmol* 2007;245:1681–1689.
- 19 van Meurs JC, Van Den Biesen PR. Autologous retinal pigment epithelium and choroid translocation in patients with exudative age-related macular degeneration: Short-term follow-up. *Am J Ophthalmol* 2003;136:688–695.
- 20 Degenring RF, Cordes A, Schrage NF. Autologous translocation of the retinal pigment epithelium and choroid in the treatment of neovascular age-related macular degeneration. *Acta Ophthalmol* 2011;89:654–659.
- 21 Stanga PE, Kychenthal A, Fitzke FW et al. Retinal pigment epithelium translocation after choroidal neovascular membrane removal in age-related macular degeneration. *Ophthalmology* 2002;109:1492–1498.
- 22 Limb GA, Daniels JT. Ocular regeneration by stem cells: Present status and future prospects. *Br Med Bull* 2008;85:47–61.
- 23 Schwartz SD, Regillo CD, Lam BL et al. Human embryonic stem cell-derived retinal pigment epithelium in patients with age-related macular degeneration and Stargardt's macular dystrophy: Follow-up of two open-label phase 1/2 studies. *Lancet* 2015;385:509–516.
- 24 Assawachananont J, Mandai M, Okamoto S et al. Transplantation of embryonic and induced pluripotent stem cell-derived 3D retinal sheets into retinal degenerative mice. *Stem Cell Rep* 2014;2:662–674.
- 25 Tucker BA, Park IH, Qi SD et al. Transplantation of adult mouse iPS cell-derived photoreceptor precursors restores retinal structure and function in degenerative mice. *PLoS One* 2011;6:e18992.
- 26 Xian B, Huang B. The immune response of stem cells in subretinal transplantation. *Stem Cell Res Ther* 2015;6:161.
- 27 Peng Y, Tang L, Zhou Y. Subretinal injection: A review on the novel route of therapeutic delivery for vitreoretinal diseases. *Ophthalmic Res* 2017;58:217–226.
- 28 Schwartz SD, Hubschman JP, Heilwell G et al. Embryonic stem cell trials for macular degeneration: A preliminary report. *Lancet* 2012;379:713–720.
- 29 Kashani AH, Lebkowski JS, Rahhal FM et al. A bioengineered retinal pigment epithelial monolayer for advanced, dry age-related macular degeneration. *Sci Transl Med* 2018;10:eaa04097.
- 30 da Cruz L, Fynes K, Georgiadis O et al. Phase 1 clinical study of an embryonic stem cell-derived retinal pigment epithelium patch in age-related macular degeneration. *Nat Biotechnol* 2018;36:328–337.
- 31 Petrus-Reurer S, Bartuma H, Aronsson M et al. Integration of subretinal suspension transplants of human embryonic stem cell-derived retinal pigment epithelial cells in a large-eyed model of geographic atrophy. *Invest Ophthalmol Vis Sci* 2017;58:1314–1322.
- 32 Tomita M, Lavik E, Klassen H et al. Biodegradable polymer composite grafts promote the survival and differentiation of retinal progenitor cells. *STEM CELLS* 2005;23:1579–1588.
- 33 Green BJ, Worthington KS, Thompson JR et al. Effect of molecular weight and functionality on acrylated poly(caprolactone) for stereolithography and biomedical applications. *Biomacromolecules* 2018;19:3682–3692.
- 34 Del Priore LV, Hornbeck R, Kaplan HJ et al. Débridement of the pig retinal pigment epithelium in vivo. *Arch Ophthalmol* 1995;113:939–944.
- 35 Burnight ER, Wiley LA, Drack AV et al. CEP290 gene transfer rescues Leber congenital amaurosis cellular phenotype. *Gene Ther* 2014;21:662–672.
- 36 Tucker BA, Scheetz TE, Mullins RF et al. Exome sequencing and analysis of induced pluripotent stem cells identify the cilia-related gene male germ cell-associated kinase (MAK) as a cause of retinitis pigmentosa. *Proc Natl Acad Sci USA* 2011;108:E569–E576.
- 37 Tucker BA, Mullins RF, Streb LM et al. Patient-specific iPSC-derived photoreceptor precursor cells as a means to investigate retinitis pigmentosa. *Elife* 2013;2:e00824.
- 38 Stone EM, Andorf JL, Whitmore SS et al. Clinically focused molecular investigation of 1000 consecutive families with inherited retinal disease. *Ophthalmology* 2017;124:1314–1331.
- 39 Burnight ER, Gupta M, Wiley LA et al. Using CRISPR-Cas9 to generate gene-corrected autologous iPSCs for the treatment of inherited retinal degeneration. *Mol Ther* 2017;25:1999–2013.
- 40 Wiley LA, Beebe DC, Mullins RF et al. A method for sectioning and immunohistochemical analysis of stem cell-derived 3-D organoids. *Curr Protoc Stem Cell Biol* 2016;37:1C.19.11–11C.19.11.
- 41 Wiley LA, Anfinson KR, Cranston CM et al. Generation of xeno-free, cGMP-compliant patient-specific iPSCs from skin biopsy. *Curr Protoc Stem Cell Biol* 2017;42:4A.12.11–14A.12.14.
- 42 Tucker BA, Anfinson KR, Mullins RF et al. Use of a synthetic xeno-free culture substrate for induced pluripotent stem cell induction and retinal differentiation. *STEM CELLS TRANSLATIONAL MEDICINE* 2013;2:16–24.
- 43 Tucker BA, Cranston CM, Anfinson KA et al. Using patient-specific induced pluripotent stem cells to interrogate the pathogenicity of a novel retinal pigment epithelium-specific 65 kDa cryptic splice site mutation and confirm eligibility for enrollment into a clinical gene augmentation trial. *Transl Res* 2015;166:740.e741–749.e741.
- 44 Worthington KS, Wiley LA, Guymon CA et al. Differentiation of induced pluripotent stem cells to neural retinal precursor cells on porous poly-lactic-co-glycolic acid scaffolds. *J Ocul Pharmacol Ther* 2016;32:310–316.
- 45 Wilson DJ, Neuringer M, Stoddard J et al. Subretinal cell-based therapy: An analysis of surgical variables to increase cell survival. *Retina* 2017;37:2162–2166.
- 46 Sohn EH, Khanna A, Tucker BA et al. Structural and biochemical analyses of choroidal thickness in human donor



eyes. *Invest Ophthalmol Vis Sci* 2014;55:1352–1360.

**47** Sarks JP, Sarks SH, Killingsworth MC. Evolution of geographic atrophy of the retinal pigment epithelium. *Eye* 1988;2:552–577.

**48** Whitmore SS, Sohn EH, Chirco KR et al. Complement activation and choriocapillaris loss in early AMD: Implications

for pathophysiology and therapy. *Prog Retin Eye Res* 2015;45:1–29.

**49** Bartuma H, Petrus-Reurer S, Aronsson M et al. In vivo imaging of subretinal bleb-induced outer retinal degeneration in the rabbit. *Invest Ophthalmol Vis Sci* 2015;56:2423–2430.

**50** Qi Y, Dai X, Zhang H et al. Transcorneal subretinal injection in mice and its

effect on the function and morphology of the retina. *PLoS One* 2015;10:e0136523.

**51** Russell S, Bennett J, Wellman JA et al. Efficacy and safety of voretigene neparvovec (AAV2-hRPE65v2) in patients with RPE65-mediated inherited retinal dystrophy: A randomised, controlled, open-label, phase 3 trial. *Lancet* 2017;390:849–860.



See [www.StemCellsTM.com](http://www.StemCellsTM.com) for supporting information available online.